JOURNAL OF APPLIED ELECTROCHEMISTRY 12 (1982) 721–734

Computerized design and evaluation of improved electrodes for lead–acid batteries

L. E. VAALER, E. W. BROOMAN

Battelle's Columbus Laboratories, Columbus, Ohio 43201, USA

H. A. FUGGITI

Exide Management and Technology Company, Yardley, Pennsylvania 19067, USA

Received

A mathematical model of a positive–negative electrode pair in a lead–acid battery has been developed, and can be solved to determine the potential and current density distribution over the electrode surfaces. With the aid of a computer the model was used to improve the grid design of the positive electrode. The results were compared with those obtained by discharging full-size electrode pairs in a laboratory cell. Agreement between projections and experimental data was about 70% with the assumptions made for certain input parameters. Further development is needed before the model can be applied to the design of 'radial' grids with curvilinear grid members.

1. Introduction

The conventional lead–acid battery grid consists of a uniform rectangular pattern of intersecting members. The paste on the grid members acts as a parallel conductor to the grid, but is a continuous rather than discrete element (as are the grids). The current collector lug is generally located near one of the top corners of the grid. The grids for the positive and negative plates are not usually mirror images of each other. When assembled into plate elements, for example, the lugs are offset from different corners. Thus, the current path between any pair of negative and positive plates enters through one lug, simultaneously spreads out through one plate and crosses through the electrolyte and separator system to the opposite plate, and converges on the second plate to its lug. Any mathematical model developed to describe and optimize this behaviour, therefore, must consider not only two-dimensional current flow in the plates but also current flow normal to these directions between the plates. A three-dimensional model is necessary to accomplish this.

There would appear to be two opportunities for improving grid design which may either allow a lighter grid to be used for a given performance, or lower the voltage drop in a grid for a given mass of lead alloy (and paste), or both. First, the conductance should be higher near the lugs since higher currents are carried here than in grid members remote from these lugs. Second, the grid members should be aligned so that the heavier, more conductive members lie in the direction of the current flow, and lighter cross-members lie in the direction of equipotential lines. Ideally the function of the latter is only to hold the structure together mechanically and aid in retaining the paste, rather than to carry any current.

We will consider in this paper* improving the distribution of grid members and the lug location in orthogonal grid designs, with some discussion of how the re-alignment of the grid elements can be accomplished.

* Based on a paper presented at the Symposium on the Electric Powered Car, AIChE, Detroit, Michigan, USA (August, 1981).

0021–891X/82/060721–14$04.18/0

2. Conceptual model

We have worked with a three-dimensional, conceptual or mathematical model, which requires no construction of prototypes and electrical measurements [1]. Models of this sort have been described by Tiedemann and Newman [2]. Euler [3], has discussed measurements on actual grids assuming, however, a uniform current density between positive and negative plates. Avoiding this assumption, which is not valid in practice, we have adopted his concept of a linear resistance network, using as a unit cell one side (half the thickness of grid and paste) of a positive and a negative grid and the separator and electrolyte between them. The grid elements are considered the resistive elements with an appropriate resistance value in parallel to represent the paste. The resistance element between electrodes is that of a rectangular cube of interelectrode length and cross-section equal to the grid area associated with each grid node. Linear polarization resistance is assumed. This assumption is better as the current density becomes more uniform, and we believe it is a good approximation for battery grids where the dispersion of current density is less than 100%.

2.1. *Methods of numerical analysis*

The current and potential distribution at each juncture of resistance elements (node) may be determined by solving Kirchoff's equation at each node. This method of modelling has been used for an unpasted lead grid assuming uniform current density [4] and for titanium electrodes in industrial electrolysis [5]. The method is equivalent to using finite difference equations to solve LaPlace's equation, with difference equations covering the internodal distances in the resistance network [6]. However, most analyses utilizing finite difference equations assume that the area or volume under consideration is divided into uniform squares or cubes with isotropic conductance. When internodal distance and specific conductance vary from element to element, the finite difference equations are more complicated.

Consider Fig. 1, which is an orthogonal, two-dimensional structure, but with different distances to the adjacent orthogonal nodes and different specific conductances in each direction. If σ' is the average conductance over Δx and σ'' that over Δy, E_0 is the potential at the centre node, and h is the distance between the centre node and an adjacent node; then:

$$\sigma' \frac{\Delta^2 E}{\Delta x^2} + \sigma'' \frac{\Delta^2 E}{\Delta y^2} = 0 \tag{1}$$

$$\sigma' \frac{\Delta^2 E}{\Delta x^2} = \left[\frac{\sigma_2(E_2 - E_0)}{h^2} - \frac{\sigma_4(E_0 - E_4)}{h_4}\right] \Big/ [\tfrac{1}{2}(h_2 + h_4)] \tag{2}$$

$$\frac{\Delta^2 E}{\Delta y^2} = \left[\frac{\sigma_3(E_3 - E_0)}{h_3} - \frac{\sigma_1(E_0 - E_1)}{h_1}\right] \Big/ [\tfrac{1}{2}(h_3 + h_1)] \tag{3}$$

$$E_0 = \frac{[(\sigma_1 E_1/h_1)(h_2 + h_4) + (\sigma_2 E_2/h_2)(h_1 + h_3) + (\sigma_3 E_3/h_3)(h_2 + h_4) + (\sigma_4 E_4/h_4)(h_1 + h_3)]}{[(\sigma_1/h_1)(h_2 + h_4) + (\sigma_2/h_2)(h_1 + h_3) + (\sigma_3/h_3)(h_2 + h_4) + (\sigma_4/h_4)(h_1 + h_3)]} \tag{4}$$

Applying Kirchoff's law to the same arrangement, we assume that the conductance associated with each element is the specific conductance of the continuum divided by the interelement distance and multiplied by half the width between nodes orthogonal to the element. Thus, for the element from 0 to 1 the conductance is:

$$C_{0,1} = (\sigma_1/h_1)(1/2)(h_2 + h_4).$$

If, by Kirchoff's law,

$$\Sigma(E_i - E_0)C_{0,i} = 0 \tag{5}$$

we again obtain Equation 4. If all values of h and σ are the same we obtain:

$$E_0 = \left(\sum_i^4 E_i\right) \Big/ 4, \tag{6}$$

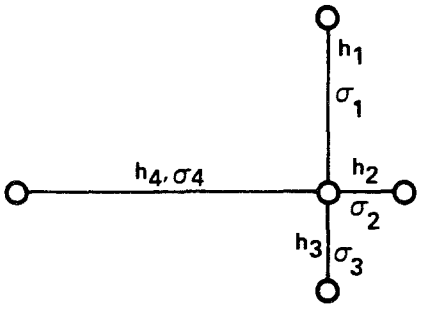

Fig. 1. Adjacent orthogonal points for calculating general finite difference equations.

which is the expression derived from finite difference equations for a uniform grid structure and medium.

Kirchoff's law appears easier to use since conductances of the lead element and the associated paste can be calculated separately and combined to give the total conductance.

2.2. *Strategy for determining potentials and currents in the linear resistance network*

2.2.1. Element conductances. Conductances were more convenient to use than resistances, since the conductance of the lead grid element and the conductance of the paste associated with it can be added to obtain the net conductance to be used in the network. The paste associated with each grid element is shown in Fig. 2. The net conductance takes into account the overpaste in excess of the grid thickness, and displacement of paste by the lead grid elements.

2.2.2. Solution of Kirchoff's equation. An equation can be written for each node of the positive and the negative grid. A typical grid array is 9 x 35 or 315 nodes per grid or a total of 630 nodes. These equations can be solved by a completely iterative procedure but we have avoided this procedure for the most part by direct solution of the simultaneous equations for each electrode.

Fig. 3 is helpful in explaining the procedure. The outer bounds of the figure define a full matrix, $2n \times 2n$, where n is the number of nodes on each plate. Quadrant I contains coefficients for the potentials at each node on the positive plate. Quadrant II contains conductances of elements between corresponding nodes on the positive and negative plate. Quadrant III contains coefficients for the negative plate and Quadrant IV repeats the values in Quadrant II. The overall matrix and each quadrant are symmetrical about diagonals. The coefficients were stored in banded matrices to reduce the memory requirements. To initiate the computations, fixed potential values were assumed at the contacts (lugs)

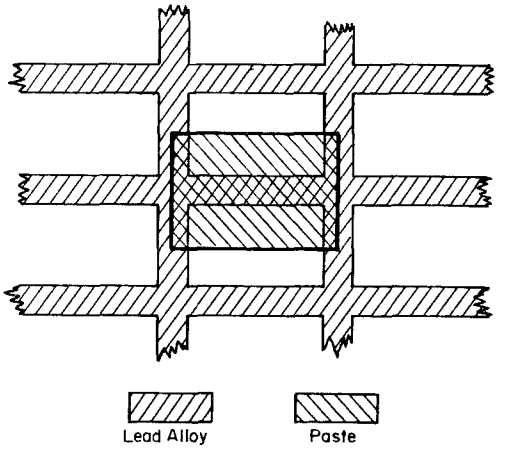

Fig. 2. Paste area associated with horizontal grid element.

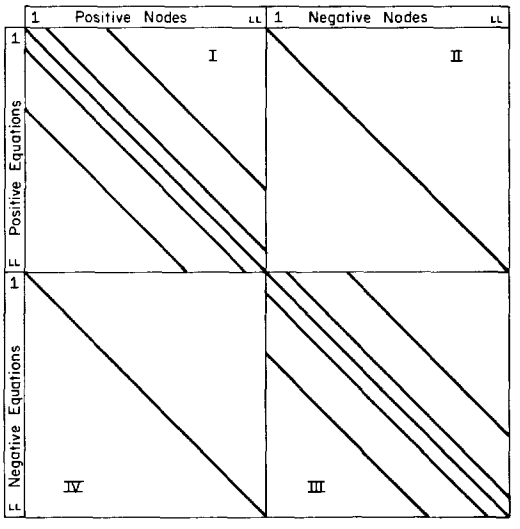

Fig. 3. Diagram of a full matrix including both positive and negative nodes.

to the positive and negative grids and for all nodes on the negative plate. Equations for the positive nodes were then solved to determine potentials at the positive nodes. These were then fixed while the equations for the negative nodes were used to calculate new potentials for these nodes. By repeating this procedure the values at both electrodes would converge after only a few (less than ten) calculations for each electrode.

2.3. *Input parameters*

2.3.1. Plate conductances. The model was first adjusted to fit an AC1GW* positive and AC2GW* negative grid pair (one side of each electrode). These grids have 35 rows (horizontal) and 10 columns (vertical), including borders. Their overall dimensions are 15.54 cm (6.12 in) wide and 16.02 cm (6.307 in) high. The thickness of the positive grid was 0.213 cm (0.084 in) and the thickness of the negative grid was 0.183 cm (0.074 in). The cross-section and the lengths of the various interior grid and border elements were estimated from enlarged, detailed drawings of the grids. The positive lug was located over the last two vertical elements and the negative lug over the first two vertical elements. The model represented the plate plugs as two parallel conductors with 2/3 of the conductance in the lug above the first (or last element) and 1/3 of the conductance in the lug above the other element.

The overpaste was assumed to be 0.0127 cm (0.005 in) total for both sides of the grid. The following values were assumed for specific conductances:

plate component	specific conductance
6% Antimony–Lead alloy	40 600 ohm^{-1} cm^{-1}
Positive paste	135 ohm^{-1} cm^{-1}
Negative paste	5496 ohm^{-1} cm^{-1}

When these values are combined with grid dimensions, the conductances were calculated for elements between the nodes as shown in Table 1.

It is evident that the lead alloy grid is the predominant current carrier in the positive plate, while the paste contributes much more significantly to the conductance in the negative plate. Therefore, a change in design to better distribute the conductance of the lead alloy should influence results more markedly on the positive than on the negative plate.

* Exide Battery Corporation.

Table 1. Conductances of grid members, associated paste, and grid–paste combination for AC1GW and AC2GW plates*

Grid member	*Conductance of positive plate AC1GW* (ohm^{-1})			*Conductance of negative plate AC2GW* (ohm^{-1})		
	Lead alloy	*Paste*	*(Lead & paste)/2*	*Lead alloy*	*Paste*	*(Lead & paste)/2*
Horizontal, internal	262.0	7.10	134.5	224.5	251.2	237.9
Horizontal, top border	1559.0	3.55	781.3	1336.0	125.7	730.9
Horizontal, bottom border	1559.0	3.55	781.3	1336.0	125.7	730.9
Vertical, internal	1372.0	95.60	733.8	1176.0	3378.0	2277.0
Vertical, left border	2464.0	47.80	1256.0	2112.0	1689.0	1901.0
Vertical, right border	4768.0	47.80	2408.0	4087.0	1689.0	2888.0
Lug	7564.0	–	3782.0	6483.0	–	3242.0

* AC1GW, AC2GW are identifying codes for Exide plates.

2.3.2. Interelectrode conductance. The resistance of the electrolyte plus separator system between the plates was assumed to be 3.72 ohm cm^2 corresponding to a conductivity of 0.2688 ohm^{-1} cm^{-2}. The area associated with a grid node is $1.68 \times 0.458 = 0.769\ cm^2$. The conductance associated with this area is 0.2067 ohm^{-1}.

3. Results of varying the grid design

3.1. *Conventional orthogonal designs*

Table 2 shows results of calculations for several grid designs and one change in lug position to the 'through-the-partition' (TTP) configuration.

Case 1 represents the AC1GW and AC2GW grid pair previously described. The voltage reported is from the positive to the negative lug and, of course, does not include the reversible cell potential but only linear resistance elements. The variation of current density has been reported three ways. The range would seem to be the least descriptive measure of dispersion. The other two figures of merit do not always show the same trend for this deterministic situation.

The potential and current density distribution of the grids may be quickly estimated visually by

Table 2. Results of calculations for orthogonal grid designs. Current 24 A, positive thickness 0.213 cm, negative thickness 0.183 cm, overpaste 0.0127 cm total for both sides

Case	*Lug arrangement*	*NCT*[a]	*Lug voltage* (V)	*Current density variation*		
				Range average	*Average absolute difference*	*Root mean squared average difference*
1	Near corners[b]	0	0.425	0.21	0.0442	0.0517
2	TTP[c]	0	0.412	0.23	0.0463	0.0543
3	Near corners	6	0.441	0.23	0.0433	0.5030
4	Near corners	12	0.459	0.24	0.0436	0.0573
5	Near corners	18	0.478	0.26	0.0512	0.0657
6	Near corners	24	0.499	0.29	0.0624	0.0772
8	Near corners	0	0.403	0.14	–	–

[a] NCT = Number of grid bars cut starting at top border.
[b] Conventional location, centre 1.7 cm from the corners.
[c] Through-the-partition configuration. Centre 4.17 cm from the centre of the plate.

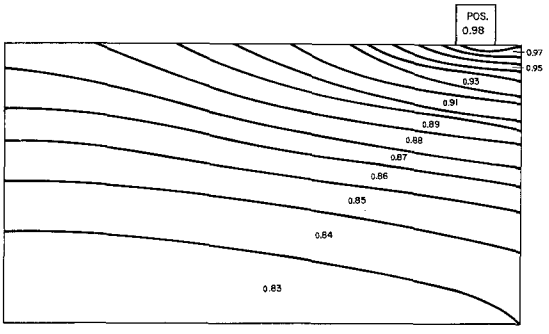

Fig. 4. Potential distribution as a fraction of total voltage drop for a positive AC1GW plate (not to scale).

plotting equal-valued lines through reduced computer printouts of the results. This approach is illustrated in Figs. 4, 5 and 6 where horizontal and vertical distances are not on the same scale. However, the higher potential drop around the tabs and the higher conductance of the negative electrode are evident.

In case 2 the centres of the positive and negative lugs have been moved from the corners inward to centres 4.17 cm (1.64 in) from the centre of the border of the plate. The closer proximity of the lugs to each other reduces the voltage drop and increases the current dispersion somewhat.

In cases 3–6 the horizontal elements in the middle of the grids were removed, forcing the current to go down into the plate. This situation was modelled to determine whether a more uniform current density would be obtained. The larger path between lugs increased the voltage and increased rather than decreased the dispersion of current density. Figs. 7 and 8 show results for case 4. The high potential drop in the positive grid around the lug causes a higher current density in this area, resulting in higher dispersion.

In case 8 the lead alloy volume of the positive plate remained the same as for case 1 but the lead alloy was re-distributed to provide more conductivity around the positive lug. The volumes of the top, bottom, and right borders were halved (the left border is already small in cross-section). The equivalent volume was transferred to interior grid members. The conductance of the interior elements is shown in Figs. 9 and 10. The lead available was arbitrarily distributed to place 25% of it in both zones I and II and 50% of it in zone III of the plate.

In zone I the cross-section assumed for the lead is greater than the volume available. Also, the only paste present is overpaste of limited capacity. Thus, this situation does not represent a practical grid design, but illustrates results with a radical distribution of the conductance. The voltage and the current density ranges were both substantially reduced.

3.2. *Modified orthogonal designs*

A grid was designed with a maximum practical pellet size and interior elements of larger cross-section.

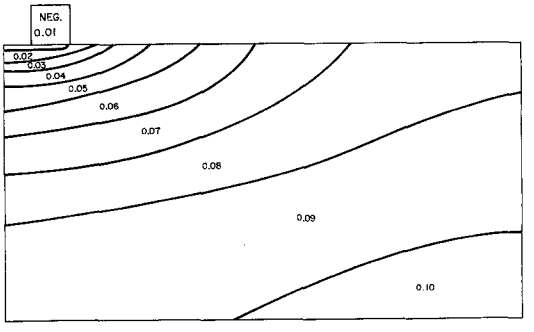

Fig. 5. Potential distribution as fraction of total voltage drop for a negative AC2GW plate (not to scale).

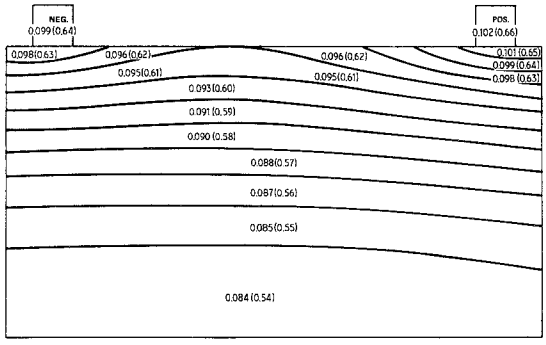

Fig. 6. Current density distribution, A cm^{-2} (A in^{-2}) for the plate pair shown in Figs. 4 and 5 (not to scale).

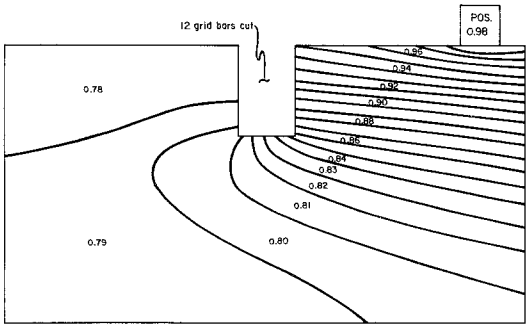

Fig. 7. Case 4 positive grid potential distribution (not to scale).

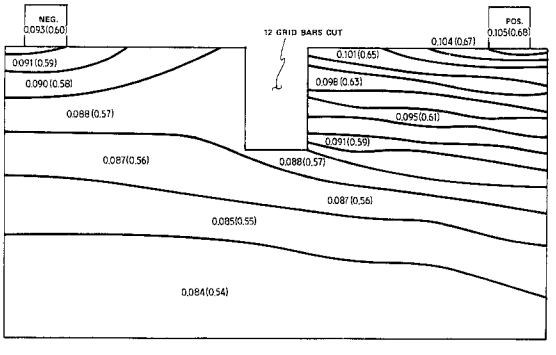

Fig. 8. Case 4 current density distribution, A cm^{-2} (A in^{-2}) for modified plates (not to scale).

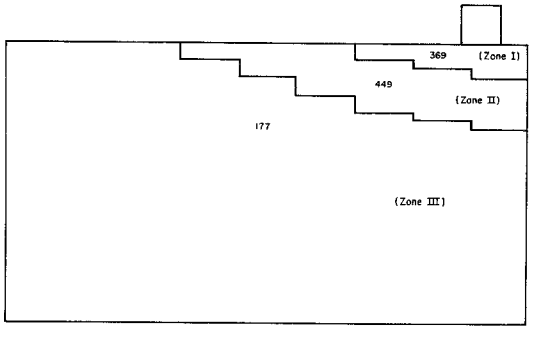

Fig. 9. Conceptual grid: conductances of horizontal elements (ohm^{-1}) (not to scale).

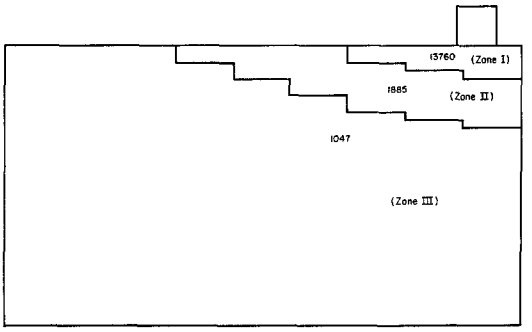

Fig. 10. Conceptual grid: conductances of vertical elements (ohm^{-1}) (not to scale).

The positive lead alloy grid was estimated to weigh 186 g and the negative 150 g, as compared to 112 g for the AC1GW positive grid.

The model was as follows:

Grid component	Dimensions
No. of columns (including borders)	11 each
No. of rows (including borders)	23 each
Thickness, positive	0.183 cm
Thickness, negative	0.147 cm
Width, positive interior member	0.183 cm
Width, negative interior member	0.147 cm
Width, bottom and side borders	0.20 cm
Width, top border	0.30 cm

Results utilizing this grid and various lug positions are shown in Table 3.

Case 9 shows that for this positive and negative grid combination the voltage is 0.451 compared with 0.412 for the AC1GW and AC2GW grid pair and the dispersion values for the current are of the order of 50% higher. The paste carried by the modified grids is less than for the thicker AC1GW positive and AC2GW negative grids so that combined conductance of paste plus lead alloy for the latter pair is greater and the IR drop through the cell less.

Table 3. Results of calculations for modified grid design. Current, 24 A. overpaste, 0.0127 cm total for both sides

Case	*Lug arrangement*[a]	*Interelectrode conductance* (ohm^{-1})	*Lug voltage* (V)	*Current density variations*		
				Range average	*Average absolute difference*	*Root mean squared average difference*
9	TTP	0.2835	0.451	0.32	0.066	0.086
10	TTP	0.2205	0.547	0.25	0.042	0.062
11	TTP	0.0840	1.247	0.088	0.020	0.024
12	POS-TOP, TTP NEG-BOT, TTP	0.2835	0.460	0.26	0.035	0.046
13	POS-TOP, Ctr NEG-BOT, Ctr	0.2835	0.475	0.28	0.036	0.047
14	POS-RT, Ctr NEG-LT, Ctr	0.2835	0.405	0.10	0.015	0.019
15	TTP	0.2835	0.409	0.16	0.032	0.038

[a] TTP = through-the-partition configurations; POS = positive plate; NEG = negative plate; TOP = top border; BOT = bottom border; RT = right border; LT = left border; Ctr = centre.

Table 4. Interelectrode conductance for various states of discharge

Specific gravity	*Acid concentration* (wt %)	*Specific conductance* ($ohm^{-1}\,cm^{-1}$)	*Interelectrode conductance* (ohm^{-1})
1.24	32.6	0.81	0.2835
1.18	25.2	0.79	–
1.11	16.1	0.63	0.2205
1.04	6.1	0.24	0.0840

Conductivity data are from [7] at 25° C.

3.2.1. Effect of state of discharge. As the battery is discharged the conductivity of the electrolyte decreases, which should increase the voltage drop in the battery but decrease the dispersion of the current. We have calculated the interelectrode conductance from the specific conductances of solutions of varying specific gravity as shown in Table 4. There is no marked change when reducing specific gravity from 1.24 to 1.18.

Cases 10 and 11 in Table 3 are for cells with specific gravities of 1.11 and 1.04, respectively, and show the anticipated changes in voltage drop and current density dispersion as the plates become discharged.

3.2.2. Effect of the position of the lugs. The relatively small effect of moving the lugs from near the plate corners to the TTP position along the top borders has been discussed. We also investigated placing the lugs on opposite sides of the grids. The effect of doing this on reducing voltage drop in two-dimensional models is well known [8]. Cases 12, 13, and 14 (Table 3) show results for three arrangements. Moving the negative lug from the top (case 9) to the bottom (case 12) increases the anticipated voltage drop slightly, but markedly decreases the current density dispersion. Centring the lugs on the top and bottom borders (case 13) has little effect as compared to case 12. Moving the lugs to the right and left borders (case 14) reduces both voltage drop and dispersion. The reason for this is that the horizontal conductance of the grid as a whole is larger than the vertical conductance due to the large number of horizontal grid members (conductors).

3.2.3. Effect of grid weight. Considering the results of variations of lug location we were interested in the effect of relocating the lugs on grid designs similar to but lighter than the AC1GW and AC2GW grids discussed previously. The design and size of the lead elements for the positive plate are shown in Fig. 11. The same design is used for the negative plate but its thickness was reduced to 0.147 cm (0.058 in). The weight of the positive lead grid is estimated to be 96 g as compared to 112 g for an AC1GW grid, and the negative plate is estimated to weigh 77 g. The lug is in the TTP position and an overpaste of 0.0127 cm (0.005 in) assumed on each side of the plate. Results for this grid pair are listed as case 15 is Table 3. The results are better than for the AC1GW–AC2GW grid pair arrangement (Table 2, case 2) even with a lead alloy weight reduction of 15%. Thus, by rotating the existing AC1GW grid design through 90 degrees, and redistributing the lead somewhat to provide better conductivity near the lug the performance can be improved with lighter grids.

4. Experimental measurements

To determine the potential distribution and voltage drop for a grid under discharge conditions a pasted AC1GW grid (positive plate) was tested in battery grade sulphuric acid electrolyte between two AC2GW pasted negative plates. The interelectrode spacing was 1.25 cm (0.5 in). Small lead wires were spot welded to specific grid nodes, the positions of which were selected from the predictions made with the

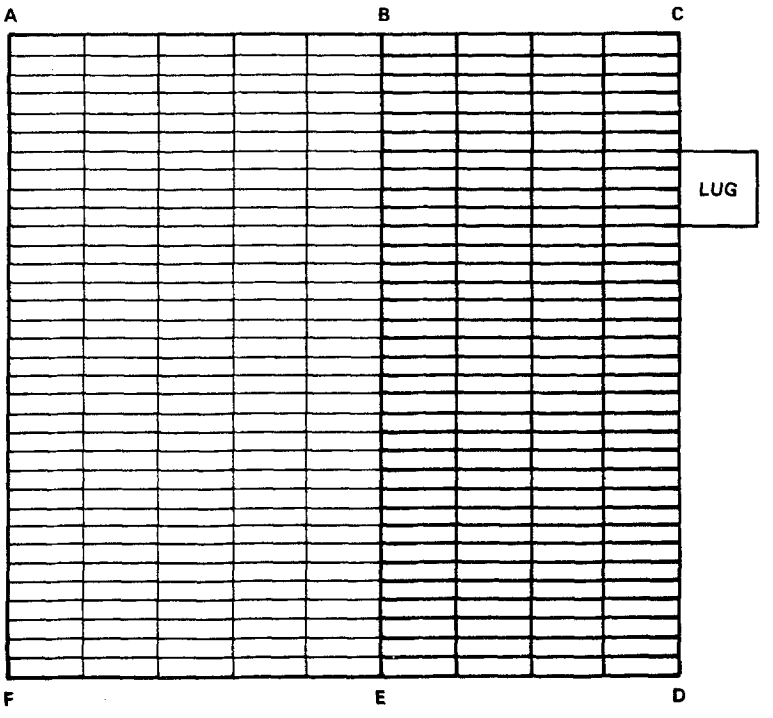

Fig. 11. Light-weight positive grid design with lug relocation. Thickness: 0.183 cm (0.072 in) Right border: 0.3 cm at tab 0.2 cm at C, D. Other borders: 0.2 cm. Horizontal elements: BCDE: 0.070 cm (0.027 in) ABEF: 0.035 cm (0.014 in). Vertical elements: BCDE: 0.073 cm (0.029 in) ABEF: 0.036 cm (0.014 in).

model. These potential probes were fixed to the grid under the paste, and protected by heat-shrinkable polyvinyl chloride tubing and an epoxy potting compound. The nodes to which the potential probes were attached are shown in Fig. 12.

The three-electrode cell was conditioned for five charge/discharge cycles as follows:

1. Charge at 2.5 A until the cell voltage reaches 2.37 V.

2. Reduce the current to 0.5 A and continue charging for the balance of 10 h. If too much gassing is observed, decrease the current, but now below 0.2 A. Record the voltage and the coulombs passed at the end of the charging period.

3. Discharge at 5.0 A to 80% depth of discharge. Record the final voltage and the coulombs passed during discharge.

The above steps were carried out four times. On the fifth cycle the cell was discharged at 10 A until the cell voltage decreased to 1.0 V. During this discharge, the continuity of the probe wires and the instruments used to measure and record the grid node potentials were checked. The purpose of this experiment was to become familiar with the monitoring technique before the desired experiments at higher discharge currents were conducted. The cell was then recharged as described above.

Starting with the fully charged cell, it was discharged for one minute at currents of 10, 25 and 50 A, respectively, without interruption, and this discharge cycle was repeated several times. Potential measurements were taken during the last half minute for each discharge current. Table 5 shows readings obtained in one experiment as well as the ratio of potentials measured at probe positions 3, 4 and 5 as compared to position 2. Table 6 compares some potential distribution data for two different positive plates used in different series of experiments. The variability in potential for individual probe positions was about 2%. The difference between the first and second series of experiments amounted to about 10%, as indicated in Table 6.

The potential measured at each node during the complete discharge cycle does not change regardless of whether the measurement is taken near the beginning or near the end of the cycle. The amount of electrolyte present is much greater than in a practical battery system so that the specific gravity changes

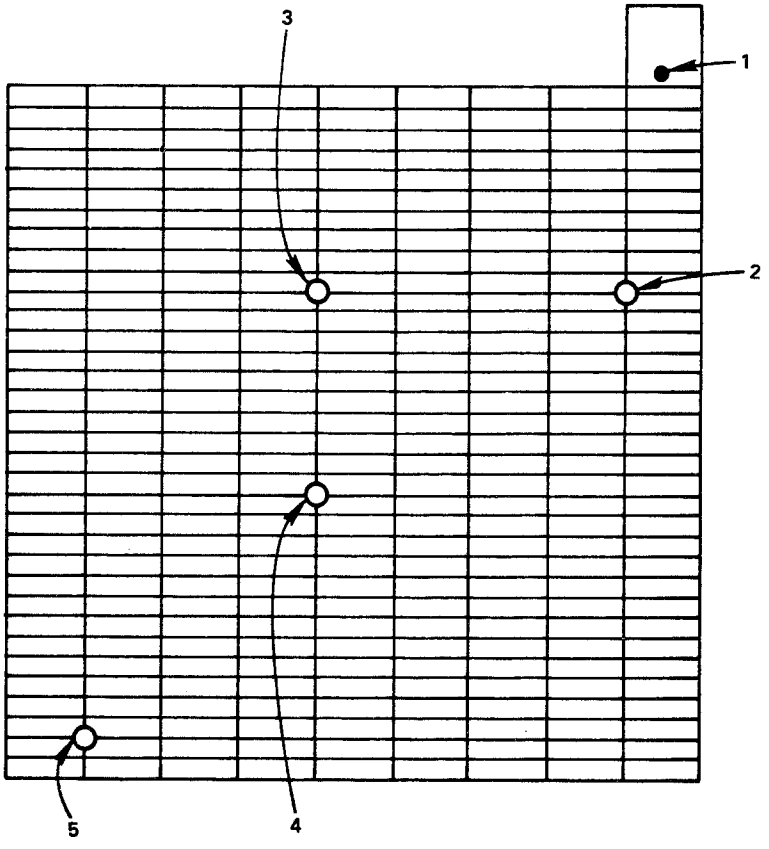

Fig. 12. Locations of probes for experimental measurements of potential during discharge.

little during discharge. The average potential drops as a function of discharge current have been plotted in Fig. 13. Plots are linear with discharge current up to 50 A, which is considered a heavy current drain for these plates (corresponds to maximum power output for electric vehicle application). Thus, there is no evidence of a selective polarization on the plate, particularly near the lug (where the current density is highest) that is sufficient to affect the linearity.

Calculated potential drops, assuming an interelectrode conductance of 0.500 ohm^{-1} between nodes (fully charged cell) are approximately 65% of those measured. This suggests that the paste conductivity is probably lower than the value assumed due to porosity, etc., in practical plates.

An independent measurement of total cell potential of a fully charged battery discharging at 5.0 A was 2.147 V. The voltage drop in excess of the reversible potential calculated for the experimental arrangement by the computer program for a 5.0 A discharge was 0.0437 V. Assuming a reversible potential of 2.10 V the total cell potential is 2.144 V, within the experimental accuracy of the measurement.

5. Conclusions

A useful mathematical model for describing the performance of grid/plate pairs has been developed for orthogonal grid designs. This model does not depend on the assumption of uniform current density distribution over each plate, but rather considers the current flow in three dimensions and projects the resulting potential distribution over the positive plate in particular, and the total voltage drop between plate pairs (positives and negatives) when the cell is being discharged at a fixed, known current. Experimental results showed that the projections and measured values were within 70% of each other. The agreement could be improved with manipulation of some of the assumed input parameters for the

Table 5. Potential drops and potential drop ratios over an AC1GW positive plate at various rates of discharge

Discharge time (min)	*Discharge current* (A)	*Position of probe on positive plate*							
		2		*3*		*4*		*5*	
		Potential drop (mV)	*Ratio**	*Potential drop* (mv)	*Ratio*	*Potential drop* (mv)	*Ratio*	*Potential drop* (mv)	*Ratio*
0.0	10	–	–	–	–	–	–	–	–
0.5	10	10.91	1.00	13.49	1.24	16.91	1.55	18.34	1.68
1.0	22	–	–	–	–	–	–	–	–
1.5	22	24.69	1.00	30.58	1.24	37.81	1.53	40.79	1.65
2.0	50	–	–	–	–	–	–	–	–
2.5	50	55.60	1.00	69.07	1.24	84.35	1.52	90.45	1.63
3.0	10	–	–	–	–	–	–	–	–
3.5	10	10.82	1.00	13.41	1.24	16.65	1.54	18.10	1.67
4.0	24	–	–	–	–	–	–	–	–
4.5	24	27.00	1.00	33.47	1.24	41.01	1.52	44.20	1.64
5.0	50	–	–	–	–	–	–	–	–
5.5	50	56.06	1.00	69.51	1.24	84.62	1.51	91.05	1.62
6.0	10	–	–	–	–	–	–	–	–
6.5	10	10.99	1.00	13.63	1.24	16.88	1.54	18.41	1.68
7.0	24	–	–	–	–	–	–	–	–
7.5	24	26.93	1.00	33.48	1.24	40.93	1.52	44.20	1.64
8.0	50	–	–	–	–	–	–	–	–
8.5	50	56.22	1.00	69.83	1.24	84.95	1.51	91.34	1.62
9.0	10	–	–	–	–	–	–	–	–
10.5	10	10.96	1.00	13.62	1.24	16.89	1.54	18.41	1.68
11.0	24	–	–	–	–	–	–	–	–
12.5	24	27.04	1.00	33.56	1.24	40.94	1.51	44.19	1.63
13.0	50	–	–	–	–	–	–	–	–
13.5	50	56.27	1.00	70.00	1.24	84.86	1.51	90.86	1.61
14.5	50	56.37	1.00	70.08	1.24	85.30	1.51	91.96	1.63
Calculated†		–	1.00	–	1.27	–	1.58	–	1.76

* Ratios are those compared to potential drop at position 2.
† Assumes a conductance of 0.500 ohm^{-1} between plates for each pellet area.

Table 6. Comparison of potential distribution data for different positive plates over two different series of experiments

Probe position	*Discharge current* (A)	*Potential measured* (mV)		*Difference* (%)
		1st series	*2nd series*	
2	10	10.96	9.8	10.6
	50	56.27	50.1	11.0
3	10	13.62	12.1	11.2
	50	70.0	62.0	11.4
4	10	16.89	15.3	9.4
	50	84.86	77.5	8.7
5	10	18.41	16.8	8.8
	50	90.86	84.8	6.7
			Average	9.7

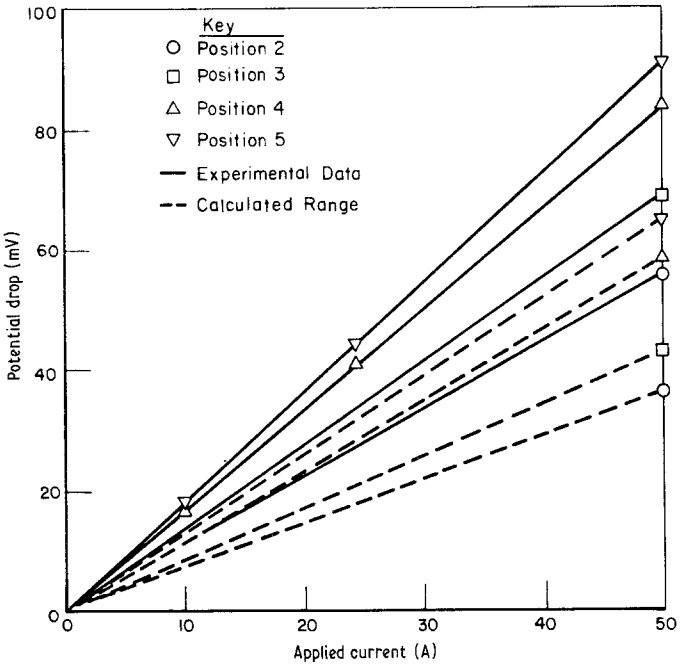

Fig. 13. Potential differences of an AC1GW positive plate during discharge. Elapsed time 3–6 min. Majority of individual data points (see Table 2) not included to facilitate presentation of data.

model. For example, the conductivity of the paste may be lower than the value selected because of inherent porosity, electrolyte occlusion, inert insulating compounds in the paste mix, and so on. However, experimental plots of potential drop in the positive plate versus discharge current were linear, as with the model. This result shows that polarization over the surface of the plate was essentially linear even at a rather high discharge rate (50 A).

The principles used to develop the conventional orthogonal grid model can be applied to the development of 'radial' grid designs; namely, non-orthogonal designs composed of linear grid members. Further development of the model is needed before radial designs with curvilinear grid members can be accommodated.

By redistributing the mass of lead such that increased current carrying capacity of the positive grid members is provided near the lug where all current flow has to leave or enter, the current density distribution over the plate can be more uniform. It is possible to plot isopotential lines and in an improved grid design the cross-section and number of grid members following these lines should be minimized. Ideally no current will flow along the isopotential lines. It then follows that the cross-sections of the grid members lying in the direction of current flow (perpendicular to the isopotential lines) should be maximized. Also, it has been shown that the location of the lugs on the grids/plates plays an important role in controlling the current distribution and minimizing the voltage drop between plate pairs. For maximum performance, the lugs should be as close to the centre of a grid border, and preferentially at the sides and not the top. However, in practical terms, the lug should be placed on the top border, and offset sufficiently to permit assembly and prevent accidently shorting. The major current carrying grid members should then be arranged in a vertical rather than horizontal manner. Horizontal grid members should provide primarily only 'structural function'. The spacings of these grid members will be controlled by lead alloy mass and optimum paste pellet size.

It has been demonstrated that IR losses due to grid design can be reduced by up to 40 mV. Translated this means that for a given mass of grid lead alloy the performance of a plate pair, hence cell, will be improved. Conversely, for a given performance the mass of lead alloy can be reduced. Specific energy density will be improved. Also, because of more uniform current density distribution, utilization of the active mass (paste) should be improved, which may correspond to a longer useful cycle life.

Acknowledgment

The work described herein was performed for the US Department of Energy under Subcontract No. 31-109-38-4207-ESB 2 managed by Argonne National Laboratory, as part of the programme on Electric Vehicle Battery Development Studies managed by George S. Hartman of Exide Management and Technology Company. The authors are indebted to the latter for his thoughful guidance and helpful suggestions and discussions during the conduct of the programme. Paul Cover, Tim Frank and Arthur Secrest of Battelle's Columbus Laboratories assisted with the experimental aspects of the programme. Ralph E. Thomas assisted in development of the mathematical model.

References

[1] L. E. Vaaler and E. W. Brooman, SAE Technical Paper Series No. 780221, Society of Automotive Engineers, Warrendale, Pennsylvania (1978).
[2] W. H. Tiedemann and J. Newman, 'Proceedings of the Symposium on Battery Design and Optimization', The Electrochemical Society, Princeton, New Jersey, Proceedings **79-1** (1979) pp. 23, 39.
[3] K. J. Euler, *Archiv für Elektrotecknik* **54** (1971) 122.
[4] W. Tiedemann, J. Newman and F. DeSua, *Power Sources* **6** (1977) 15.
[5] L. E. Vaaler, *J. Appl. Electrochem.* **9** (1979) 21.
[6] J. A. Klingert, S. Lynn and C. W. Tobias, *Electrochim. Acta* **9** (1964) 297.
[7] A. N. Campbell, E. M. Kartymark, D. Bisset and M. E. Bednas, *Can. J. Chem.* **31** (1953) 30515.
[8] P. M. Robertson, *Electrochim. Acta* **22** (1977) 411.